Optics and Lasers in Engineering 115 (2019) 53–58

Contents lists available at ScienceDirect

Optics and Lasers in Engineering

journal homepage: www.elsevier.com/locate/optlaseng

Fabrication of 2D thin-film filter-array for compressive sensing spectroscopy

Cheolsun Kim, Woong-Bi Lee, Soo Kyung Lee, Yong Tak Lee, Heung-No Lee*

School of Electrical Engineering and Computer Science, Gwangju Institute of Science and Technology, Gwangju 61005, South Korea

ARTICLE INFO

Keywords:
Spectroscopy
Thin films
Inverse problems
Compressive sensing

ABSTRACT

We demonstrate 2D filter-array compressive sensing spectroscopy based on thin-film technology and a compressive sensing reconstruction algorithm. To obtain different spectral modulations, we fabricate a set of multilayer filters using alternating low- and high-index materials and reconstruct the input spectrum using a small number of measurements. Experimental results show that the fabricated filter-array provides compatible spectral resolution performance with a conventional spectrometer in monochromatic lights and LEDs. In addition, the fabricated filter-array covers a wide range of wavelengths with a single exposure.

1. Introduction

The demand for spectrum information is increasing not only in research and development but also in the private sector. In response to this demand, researchers are trying to make spectrometers that are both small and inexpensive. These spectrometers could be used in various fields, such as medical systems, mobile applications, and remote sensing [1–3]. In particular, optical filter-based spectrometers do not need motorized or dispersive elements, and their filter-array can be directly attached to the detectors so that they can be easily miniaturized. However, there is a trade-off between size (for integrating filters) and spectral resolution with miniaturized spectrometers.

Over the years, numerous approaches to applying compressive sensing (CS) techniques have been proposed to reduce the size of spectroscopes without reducing spectral resolution, or potentially even improving it. These approaches [4–7] include the following: band pass filters [4], random transmittance filters [5], photonic crystal slabs [6], and liquid crystal phase retarders [7]. Recently, Fabry–Perot (FP)-based CS spectroscopy methods have been presented [8,9]. To acquire differently modulated spectral measurements, a 2D array of FP resonators with different cavity depths has been tried [8] as well as a piezo-actuated device that changes the distance between two FP mirrors has been tried [9]. A hundred FP resonators are used to recover the input spectrum in [8], and the operational range of the piezo-actuator imposes mechanical limitations in [9].

The CS framework [10–12] is an efficient sampling and reconstruction scheme that requires fewer samples to reconstruct the signal than that required by conventional sampling. The CS framework can be applied to filter-based spectroscopy, offering the advantage of reducing the number of filters and detectors required and allowing the system to be miniaturized.

In spectroscopy, the relation between the spectral components of the input light source $\mathbf{x} \in \mathbb{R}^{N\times 1}$ and the modulated signal $\mathbf{y} \in \mathbb{R}^{M\times 1}$ can be expressed as follows:

$$\mathbf{y} = \mathbf{T}\mathbf{x}, \tag{1}$$

where $\mathbf{T} \in \mathbb{R}^{M\times N}$ is the sensing matrix. Each row of the sensing matrix is to represent the transmission function (TF) of i-th filter, $\boldsymbol{T}_m \in \mathbb{R}^{1\times N}$ for $m = 1, 2, \ldots, M$. In order to achieve miniaturization of spectroscope without degradation of spectral resolution, the CS framework is utilized in spectroscopy, where the number of filters is set to be smaller than the number of spectral components ($M < N$). Then, Eq. (1) becomes an underdetermined linear system. A sparse signal reconstruction algorithm with $L1$ norm minimization can be used to solve Eq. (1), if the input spectrum is either naturally sparse or can be sparsely represented in some basis $\mathbf{\Phi} \in \mathbb{R}^{N\times N}$, i.e., $\mathbf{x} = \mathbf{\Phi}\mathbf{s}$, where $\mathbf{s} \in \mathbb{R}^{N\times 1}$ is a sparse vector. Then, Eq. (1) becomes

$$\mathbf{y} = \mathbf{T}\mathbf{\Phi}\mathbf{s} \tag{2}$$

The sparse signal $\mathbf{s}$ can be estimated by solving the following $L1$ norm minimization problem:

$$\hat{\mathbf{s}} = \arg\min_{\mathbf{s}} \|\mathbf{s}\|_1 \text{ subject to} \|\mathbf{y} - \mathbf{T}\mathbf{\Phi}\mathbf{s}\|_2 \leq \varepsilon \tag{3}$$

where ε is a small non-negative constant. The reconstructed input spectrum $\hat{\mathbf{x}}$ is then $\mathbf{\Phi}\hat{\mathbf{s}}$.

In this paper, we demonstrate 2D filter-array CS spectroscopy. This uses a multilayer thin-film filter-array for spectral modulation, where each filter modulates the input spectrum using different sensing patterns. A CMOS image camera reads out the modulated signals with a

* Corresponding author.
E-mail address: heungno@gist.ac.kr (H.-N. Lee).

https://doi.org/10.1016/j.optlaseng.2018.10.018
Received 22 February 2018; Received in revised form 2 October 2018; Accepted 31 October 2018

Table 1
Recursion for calculating reflection coefficients.

Input: $\lambda, \theta_1 = 0$, $\boldsymbol{n} = \{n_1, n_2, \cdots, n_{l-1}, n_l\}$, $\boldsymbol{d} = \{d_2, d_3, \cdots, d_{l-1}, d_l\}$.

Step 1: Obtain θ_k, β_k, and N_k
$\theta_k = \sin^{-1}(\frac{n_{k-1}}{n_k} \sin\theta_{k-1})$, $for\ k = 2,\ 3,\ \cdots,\ l$.
$\beta_k = 2\pi \cos(\theta_k) n_k d_k / \lambda$, $for\ k = 2,\ 3,\ \cdots,\ l$.
$N_k = \begin{cases} n_k/\cos\theta_k & for\ TE \\ n_k \cos\theta_k & for\ TM \end{cases}$, $for\ k = 1,\ 2,\ \cdots,\ l$.
Step 2: Set $\eta_l = N_l$
Step 3: Obtain η_2
Decrement k by 1 from $l-1$ to 2
$\eta_k = N_k \frac{\eta_{k+1}\cos\beta_k + jN_k \sin\beta_k}{N_k \cos\beta_k + j\eta_{k+1}\sin\beta_k}$
return η_2
Step 4: Compute $\rho = (N_1 - \eta_2)/(N_1 + \eta_2)$.

Output: ρ

single exposure, and then a reconstruction algorithm is applied that depends on the modulated signals and the sensing matrix, allowing the input spectrum to be recovered.

The research focus has been given to fabrication of the multilayer thin-film filters for actual CS spectroscopy implementation and verification experiments. For fabricating as a 2D filter-array, we use commonly available materials SiNx and SiO2 for high and low refractive index materials which are deposited alternately on the substrate with varying thicknesses. Furthermore, we come up with a practical way that set of filters can be deposited on a single substrate with different thicknesses of layers.

2. 2D filter-array

2.1. Multilayer thin-film filter

Thin films are a basic component that have been applied in a variety of areas, including semiconductor devices, optical coatings, and solar cells [13]. The theoretical TF of a multilayer thin-film filter is given by [14]

$$T(\lambda, \theta_1) = 1 - \tfrac{1}{2}\left(|\rho_{TE}|^2 + |\rho_{TM}|^2\right), \tag{4}$$

where ρ_{TE} and ρ_{TM} are the reflection coefficients. Given a wavelength λ and the incident angle θ_1, TF can be calculated using recursive routines shown in Table 1.

In Table 1, given the input of a wavelength λ, a vector of l refractive indices $\boldsymbol{n} = (n_1, n_2, \cdots, n_{l-1}, n_l)$ and a vector of $l-1$ layer thicknesses $\boldsymbol{d} = (d_2, d_3, \cdots, d_{l-1}, d_l)$, a reflection coefficient ρ is generated. Note that there are l layers considered in total. The first one is the layer of the air and the last one is the layer of the substrate. The light is assumed to be arriving from the air to the second layer in normal incidence. The first index n_1 in the vector $\boldsymbol{n}$ represents the refractive index of the air. The last one n_l in the vector $\boldsymbol{n}$ represents the refractive index of the substrate. The refractive indices of the intermediate thin-film layers are denoted by n_2 to n_{l-1}. The thickness of the air does not need to be considered. The thickness of the substrate is denoted by d_l.

The thicknesses of the intermediate thin-film layers are denoted by d_2 to d_{l-1}. The incidence angle of the light passing from the kth to the $k+1$th layer is θ_k, and η_k is the effective complex-valued index of the kth layer. A TF for a single filter is obtained by considering all wavelengths in the range of interest. An array of TFs for the M filters can be obtained by repeating this process where each filter $\boldsymbol{T}_m \in \mathbb{R}^{1\times N}$ for $m = 1,\ 2, \cdots, M$ in Eq. (1) is generated from a unique set of refractive index and thickness vectors.

2.2. Numerical design of 2D filter-array

To implement the proposed 2D filter-array, we numerically modeled the proposed spectroscopy method with reference to [14–16], and according to the following steps. (i) Generate the reference vector of layer thicknesses, i.e. $\boldsymbol{d} = (d_2, d_3, \cdots, d_{l-1}, d_l)$, for the reference filter. (ii) Generate a vector of thicknesses for the other filter by randomly removing one to five layer thicknesses from the reference vector. (iii) Repeat the step (ii) 35 times to create a total of 36 vectors of thicknesses. (iv) Use the recursion Table 1 and Eq. (4) to calculate the TFs for a new filter-array (sensing matrix). (v) Use the mutual coherence μ to quantify the goodness of the sensing matrix of the designed filter-array. Mutual coherence μ is defined as $\mu \triangleq \max_{i,j} |o_{ij}|$, where o_{ij} is the (i, j)th off-diagonal element of the Gram matrix, $\mathbf{T}^*\mathbf{T} \in \mathbb{R}^{N\times N}$. $\mathbf{T}^*$ denotes the conjugate transpose of $\mathbf{T}$. With these steps, we can generate a single set of 36 filters. By repeating these steps, multiple sets of 36 filters can be obtained. Among these sets of filter-arrays, the set of filters with a smallest mutual coherence is selected.

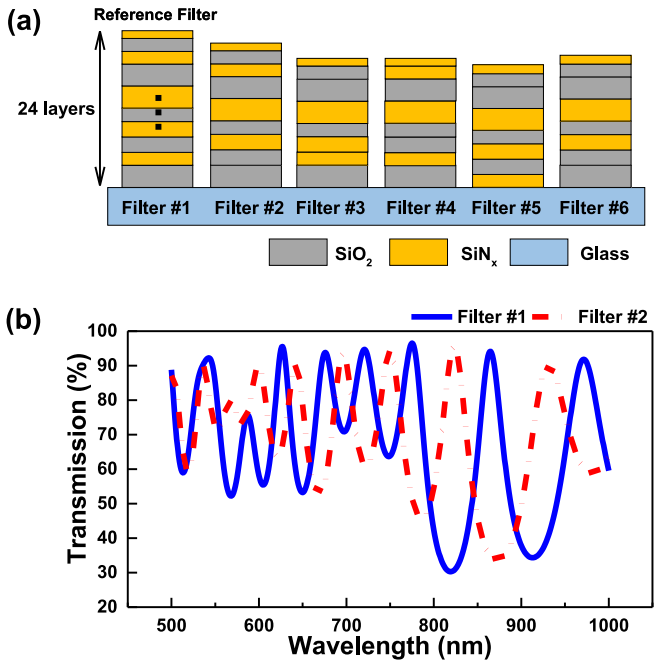

Fig. 1. (a) Schematic of the thin-film filter-array. (b) Example of two transmission functions for thin-film filters.

In CS framework, a sensing matrix with a smaller mutual coherence is better than the one with a higher mutual coherence to capture the information of input signal to be reconstructed [5,17]. A schematic of the proposed filter-array is shown in Fig. 1(a). Each time a layer is removed, the layers above and those below come together to form a single layer with two thicknesses added up. We consider two materials, SiN_x and SiO_2 for the high- and low-refractive index materials with refractive indices of 2.02 for SiN_x and 1.45 for SiO_2. The thickness range of each layer is from 50 to 150 nm. Through the numerical design, we empirically found that removal of up to five layers from the 24-layer reference filter was possible to create a 6×6 filter-array with a low coherence.

Fig. 1(b) shows the TFs for two designed filters as examples. In conventional spectroscopy, the TFs with a large spectral depth and a narrow spectral peak are preferred in order to prevent interference among measurements. In compressive sensing spectroscopy, Each TF of the filter should be wide enough so that the set of the small number of filters fully senses the spectral information in the given wavelength range [9].

Each filter shows several spectral peaks and rapid changes of transmission value with respect to wavelength. Therefore, each filter has a high optical throughput that the energy (intensity) which passes through the filter is higher than that with the conventional bandpass filter approach. In addition, fewer filters can be used to cover the entire wavelength range with the proposed method. For example, suppose 250 bandpass filters are used to cover the wavelength range from 500 to

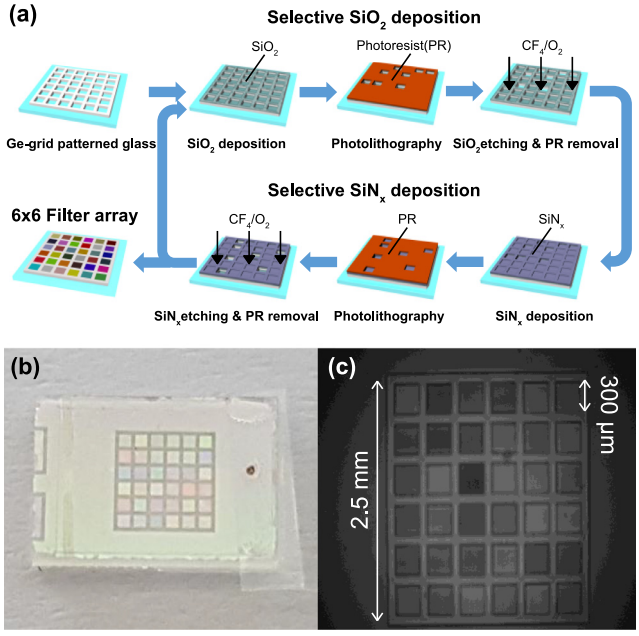

Fig. 2. (a) Schematic of the thin-film filter-array fabrication process. (b) Photograph of a fabricated thin-film filter-array. (c) Monochrome image of the thin-film filter-array taken at a wavelength of 700 nm.

1000 nm. Then, the bandwidth of TF is 2 nm, according to the conventional bandpass filter design. In the proposed approach, the same range of wavelength can be covered with only 36 proposed filters, subject to the use of a recovery algorithm present at the reconstruction end.

2.3. Filter-array fabrication

Fig. 2(a) shows the process in which a thin-film filter-array is fabricated. This comprises two main parts; one is SiO_2 film deposition and the other is SiN_x film deposition according to the specified thicknesses. Prior to depositing an SiO_2 film, a 6×6 germanium (Ge) grid with elements of size 300 μm and spacing 100 μm was formed on the glass using an e-beam evaporator to separate the filters. In this grid, SiO_2 and SiN_x layers were deposited with the width of 300 μm in each filter. Then, selective deposition was done as follow: An intentionally thick SiO_2 film was deposited on the glass patterned with the Ge grid using plasma- enhanced chemical vapor deposition. The regions where the film should not be deposited were then removed by conventional photolithography, namely CF_4/O_2 reactive ion etching. The process pressure and radio- frequency power were maintained at 50 mTorr and 50 W, respectively. The SiN_x film deposition process was performed in the same manner as for SiO_2. Finally, these two main steps, SiO_2 and SiN_x film deposition, were repeated 12 times each to lay down 24 layers. Fig. 2(b) and (c) show a photograph of a fabricated thin-film filter-array and a monochrome image of the filter-array, respectively. Each filter is composed of a different number of layers each with different thicknesses; therefore, each one has unique color due to its different TF, as shown in Fig. 1(b).

3. Experiments

3.1. Experimental setup

Optical setups for experimental verification of the proposed spectroscopy system are shown in Fig. 3. Fig. 3(a) depicts the optical setup for measuring TFs of a filter-array. The setup for testing the performance of the proposed system is shown in Fig. 3(b). The photographs of the optical setup and the CMOS image camera with the thin-film filter-array

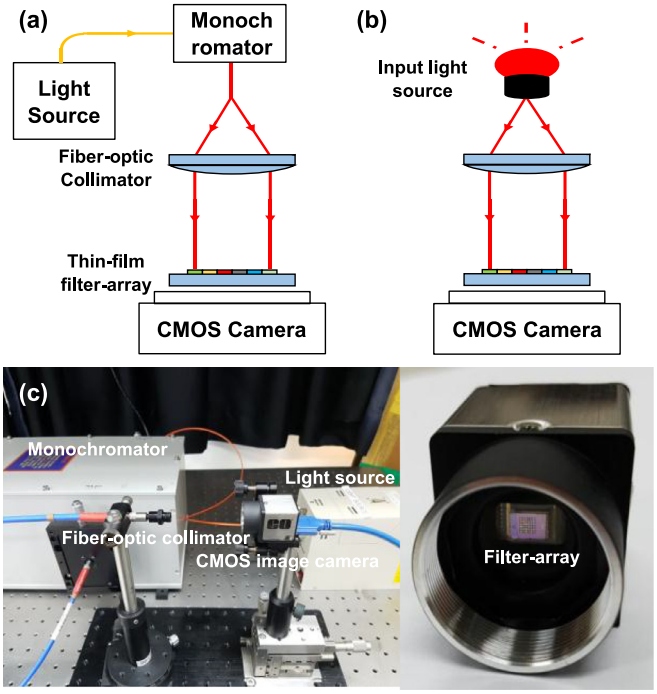

Fig. 3. (a) Schematic of the optical setup for measuring the sensing matrix. (b) Schematic of the optical setup for testing the performance of the proposed spectroscopy system. (c) Photographs of the optical setup and the CMOS image camera with the thin-film filter-array.

are shown in Fig. 3(c). During the optical experiments, we set the incident angle to filter-array as normal incidence. Using a linear stage, a rotational stage and optical mounting posts, we aligned the optical fiber with the CMOS image camera (E0-1312, Edmund Optics) for the normal incidence.

In Fig. 3(a), a halogen lamp (KLS-150H-LS-150D, Kwangwoo) was used to provide a continuous light spectrum. It was put into a monochromator (MMAC-200, Mi Optics) to produce a specific narrow wavelength band. Then, a fiber-optic collimator was used to form a beam of parallel light. The beam was fed into the CMOS image camera through the fabricated thin-film filter-array. With a single exposure, each filter modulated the light in a different pattern. The modulated light was read out by pixels of CMOS image camera, yielding $M = 36$ distinct output signals $\mathbf{y}$ in Eq. (1). Each output signal was taken by summing up the modulated values of the pixels underneath the pertinent filter.

To apply CS reconstruction algorithms to the proposed system, the sensing matrix $\mathbf{T}$ must be pre-determined. Let us denote the intensity which passes through the filter-array as $IF(m, \lambda)$ and the intensity without the filter-array as $IWF(m, \lambda)$, where m is the filter index and λ is the wavelength. The sensing matrix is then given by

$$T(m,\lambda) = \frac{IF(m,\lambda) - BI(m,\lambda)}{IWF(m,\lambda) - BI(m,\lambda)}, \tag{5}$$

where $BI(m, \lambda)$ is the background intensity. We took 500 wavelength samples, spaced 1 nm apart, in the range from 500 to 1000 nm. The measured sensing matrix $\mathbf{T} \in \mathbb{R}^{36 \times 500}$ obtained from the fabricated thin-film filter-array is shown in Fig. 4. Each TF of the filters, a row of the color map, is shown as a combination of colors, i.e., red (high transmission value) and blue (low transmission value). Different TFs show different places of high and low transmission values indicating mutual uncorrelation. As a set of 36 filters, the filter-array covers the entire wavelength range with high optical throughput.

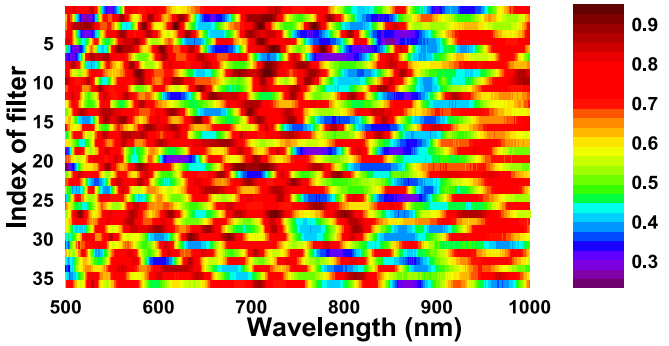

Fig. 4. Color map of the measured sensing matrix for the thin-film filter-array. Each row represents the TF of a filter with respect to wavelength.

3.2. Computational experiments

To quantify the performance and explore the two-point resolution of the fabricated filter-array, we conducted computational experiments. The two-point resolution is the ability to distinguish the spectral peaks which are closely spaced. For the experiments, we generated mono-peak spectra and two-peak spectra as input spectra using the Gaussian function. A generated input spectrum $\mathbf{x}$ was numerically modulated by multiplying the measured sensing matrix $\mathbf{T}$ as shown in Eq. (1). Then, using the M-modulated signals (measurements) and the sensing matrix $\mathbf{T}$, a reconstruction algorithm is used to recover the input spectrum. In the experiments, we considered that the input spectrum was a directly sparse signal. The mean-squared error (MSE) between the input spectrum $\mathbf{x}$ and the reconstructed spectrum $\hat{\mathbf{x}}$ was calculated. The MSE is defined as $\|\mathbf{x}-\hat{\mathbf{x}}\|_2^2/N$.

We firstly tested the spectral reconstruction performance of the fabricated filter-array with changing the full width at half maximum (FWHM) of the generated input signals. We made three noisy environments by adding the additive noise $\mathbf{n}$ to Eq. (1) as $\mathbf{y}=\mathbf{T}\mathbf{x}+\mathbf{n}$ whose the signal to noise ratios (SNRs) were 20, 25, 30 dB. The SNR in decibels is defined as $10\cdot\log_{10}(\|\mathbf{x}\|_2^2/N\sigma^2)$, where σ is the standard deviation of the noise.

The spectral reconstruction performances with respect to the FWHMs are shown in Fig. 5(a). For the two-peak spectrum, the distance between two peaks was determined as $[1.5\cdot\mathrm{FWHM}]$, where $[\cdot]$ is the nearest integer function. We averaged all the MSEs of the spectrum over the peak-locations from 500 to 999 nm in a given FWHM. As shown in Fig. 5(a), the mono-peak spectrum is reconstructed better than two-peak spectrum. As the FWHM increased, the performance of spectral reconstruction is degraded. This is due to the increased sparsity of the spectrum.

Second, we verified the stability of noise along the SNR conditions for the fabricated filter-array. As shown in Fig. 5(b), the reconstruction performance on mono-peak spectrum is better than that of the two-peak spectrum. In addition, when the FWHM is 1 nm, the reconstruction performance is better than the FWHM with 2 nm. Despite the additive noise, the results show that the fabricated filter-array is robust to the noisy environments.

As depicted in Fig. 5, the reconstruction performance of the fabricated filter-array depends on the FWHM and the SNR. For the two-point resolution, the MSE has the smallest value when the FWHM of the two-peak spectrum is 1 nm. The overall MSEs are small enough to use the fabricated filter-array to conduct the optical experiments.

3.3. Optical experiments

Optical experiments were then conducted to evaluate the performance of the proposed system, as shown in Fig. 3(b). Narrow-band monochromatic lights and LEDs were used as input light sources. To generate narrow-band light, a supercontinuum white light source (SuperK COMPACT, NKT Photonics) was placed in the monochromator, making a narrow band of light with a full width at half maximum (FWHM) of approximately 1 nm. These light sources were fed into the CMOS image camera through the filter-array, simultaneously capturing the M differently modulated signals. The M-modulated signals and the measured sensing matrix $\mathbf{T}$ were then used to solve Eq. (3). We used a Gaussian kernel matrix as the sparsifying basis $\mathbf{\Phi}$. The spectral waveform can be represented as a linear combination of Gaussian kernels, and a Gaussian kernel can be easily generated with two parameters, namely the peak location and the FWHM value [4,18]. The *l1_ls_noneg* algorithm [19] was used as a reconstruction algorithm to solve Eq. (3) with non-negativity constraints.

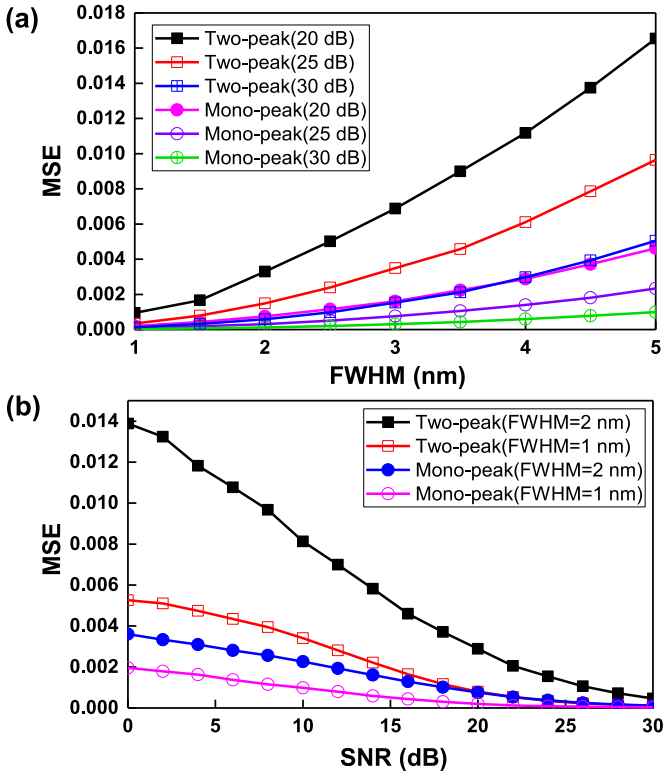

Fig. 5. (a) Computational reconstruction performance of the fabricated thin-film filter-array with respect to the FWHM. (b) Computational spectral reconstruction performance of the fabricated thin-film filter-array with respect to the SNR.

Fig. 6 shows the reconstruction results for monochromatic lights and LEDs. For comparison, the reference spectrum and the reconstructed spectrum were normalized to the range between zero and one.

The optical experimental results for monochromatic lights are shown in Fig. 6(a). In our optical experiment, depicted in Fig. 3(c), we use four different monochromatic spectra, with spectral peaks located at 600, 700, 800, and 900 nm, respectively. The reference spectra are measured using an optical spectrum analyzer (AQ-6315B, Ando) which indicate actual spectral peak locations at 598.7, 700.4, 800.5, and 900.4 nm, respectively. Using the fabricated filter-array CS spectroscopy with the reconstruction algorithm, the spectral peak locations are reconstructed at 599, 699, 799, and 901 nm, respectively. The mean FWHM of the reference spectra is approximately 1 nm, and the mean FWHM for the reconstructed spectra is approximately 1.4 nm.

Fig. 6(b) shows the spectral reconstructions of green (527 nm) and red (635 nm) LEDs. For the reference spectra, we measure the LEDs using a grating spectrometer (QE65000, Ocean Optics). The spectral peak locations for the reference LEDs are 527.6 nm (green LED) and 634.9 nm

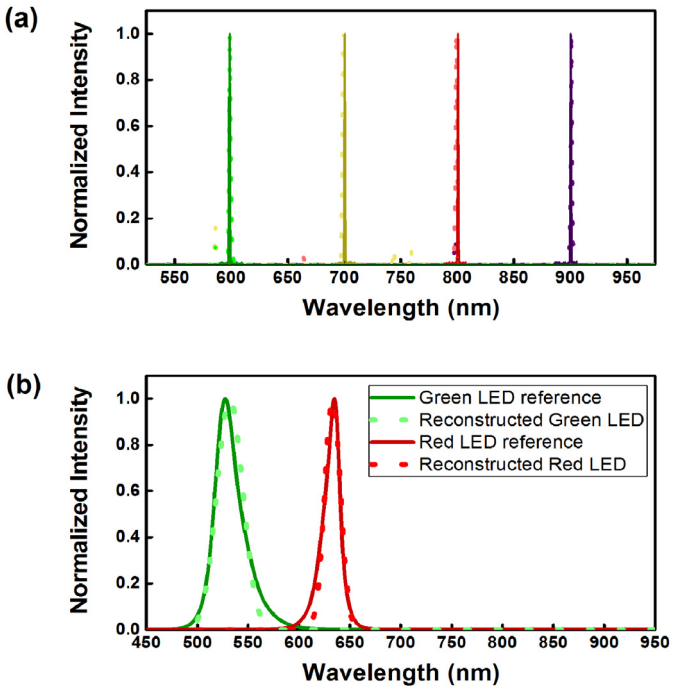

Fig. 6. Spectral reconstructions of several different input light sources. (a) Spectral reconstructions of monochromatic lights (dots) compared with reference spectra (solid lines): 600 nm (green), 700 nm (yellow), 800 nm (red), and 900 nm (purple). (b) Spectral reconstructions of LEDs (dots) compared with reference spectra (solid lines): green LED (527 nm), and red LED (635 nm).

(red LED), and the reconstructed spectral peak locations are 531 nm (green LED) and 633 nm (red LED). The peak signal-to-noise ratios are 28.3 dB (green LED) and 31.7 dB (red LED).

Discussing Fig. 6, the spectra of reconstructed monochromatic lights show several negligible spikes. This is probably due to background noise in the optical experiments. But overall, the reconstruction results of the proposed CS spectroscopy system for monochromatic lights and LEDs are similar to those of the grating spectrometer. Furthermore, the number of modulated signals is significantly small ($M = 36$) that the measurement to wavelength sample ratio is 36:500 (ratio between M and N).

To further explore the performance of the proposed CS spectroscopy, we conducted the computational experiment on the fabricated filter-array using a continuous light source, halogen lamp. For the experiment, we used the measured sensing matrix**T**. The conventionally measured spectrum of the halogen lamp was used as the input spectrum **x**. The modulated signals were generated by numerically multiplying the sensing matrix and the input spectrum. By solving Eq. (3), we reconstructed the continuous spectrum of light. In Fig. 7, we present computational spectral reconstruction of the halogen lamp. The peak signal-to-noise ratio is 43.8 dB. Due to the limitations of our optical components to reject the spectrum of the halogen lamp except for the wavelength range from 500 to 1000 nm, we could not perform the optical experiment on the continuous source. However, the computational reconstruction result of the halogen lamp indicates that the fabricated filter-array can be utilized for recovering the various kinds of spectra in the given wavelength range without limitations of the optical components.

Fabricating the proposed filter-array can be more difficult than fabricating Fabry–Perot structure due to the large number of layers for the proposed filter-array. However, the proposed spectroscope is compact and it does not need motorized components which were used with the Fabry–Perot structure [9]. In addition, thanks to the 2D array structure, the proposed spectroscope captures all measurements in a single exposure. But the Fabry–Perot spectroscope [9] required a number of

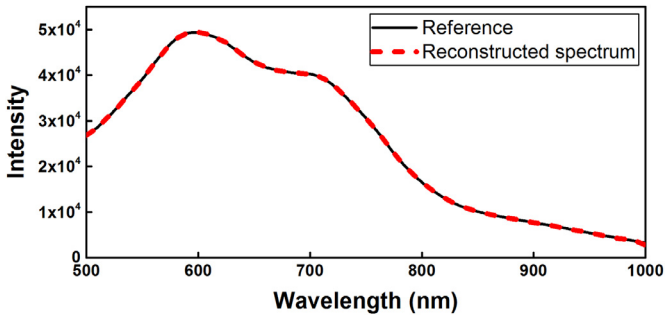

Fig. 7. Computational spectral reconstruction of a halogen lamp (red dash line) compared with the reference spectrum (black solid line) measured by a conventional spectrometer.

exposures as many times as the number of measurements. Compared to Fabry–Perot spectroscope [8], the proposed spectroscope utilizes 36 filters to cover the wavelength range from 500 to 1000 nm, but 100 filters were used in [8] to cover the range from 500 to 750 nm.

4. Conclusion

We have demonstrated a 2D array CS spectroscope based on thin-film technology. A 2D thin-film filter-array is fabricated based on array processing. Using the fabricated filter-array, measurements are obtained to which the CS reconstruction algorithm is applied. Finally, demonstration of input spectrum reconstruction is successfully made. The proposed system is compact, portable, and obtains the necessary measurements in a single exposure thanks to its structural advantages. Moreover, it works over a wide spectral range, from the visible light region to the near-infrared region. Compared with conventional spectrometers (non-CS spectrometers), the proposed system has a high optical throughput and compatible spectral resolution performance in monochromatic lights and LEDs with significantly less number of measurements.

Acknowledgments

This work was supported by the National Research Foundation of Korea (NRF) grant funded by the Korean government (MSIP) (NRF-2018R1A2A1A19018665).

References

[1] Bacon CP, Mattley Y, DeFrece R. Miniature spectroscopic instrumentation: applications to biology and chemistry. Rev Sci Instrum 2004;75:1–16.
[2] Kim S, Cho D, Kim J, Kim M, Youn S, Jang JE, et al. Smartphone based multispectral imaging: system development and potential for mobile skin diagnosis. Biomed Opt Express 2016;7:5294–307.
[3] Clark RN, Roush TL. Reflectance spectroscopy: quantitative analysis techniques for remote sensing applications. J Geophys Res Solid Earth 1984;89:6329–40.
[4] Oliver J, Lee W, Park S, Lee H-N. Improving resolution of miniature spectrometers by exploiting sparse nature of signals. Opt Express 2012;20:2613–25.
[5] Oliver J, Lee W-B, Lee H-N. Filters with random transmittance for improving resolution in filter-array-based spectrometers. Opt Express 2013;21:3969–89.
[6] Wang Z, Yu Z. Spectral analysis based on compressive sensing in nanophotonic structures. Opt Express 2014;22:25608–14.
[7] August Y, Stern A. Compressive sensing spectrometry based on liquid crystal devices. Opt Lett 2013;38:4996–9.
[8] Huang E, Ma Q, Liu Z. Etalon array reconstructive spectrometry. Sci Rep 2017;7.
[9] Oiknine Y, August I, Blumberg DG, Stern A. Compressive sensing resonator spectroscopy. Opt Lett 2017;42:25–8.
[10] Donoho DL. Compressed sensing. IEEE Trans Inf Theory 2006;52:1289–306.
[11] Baraniuk RG. Compressive sensing [lecture notes]. IEEE Signal Process Mag 2007;24:118–21.
[12] Qaisar S, Bilal RM, Iqbal W, Naureen M, Lee S. Compressive sensing: from theory to applications, a survey. J Commun Netw 2013;15:443–56.

[13] Macleod HA. Thin-film optical filters. CRC press; 2001.
[14] Barry JR, Kahn JM. Link design for nondirected wireless infrared communications. Appl Opt 1995;34:3764–76.
[15] Pedrotti FL, Pedrotti LS. Introduction to optics. 2nd ed. Prentice Hall; 1993.
[16] Topasna DM, Topasna GA. Numerical modeling of thin film optical filters. Proc. SPIE 2009;9666:96661P.
[17] Candes EJ, Eldar YC, Needell D, Randall P. Compressed sensing with coherent and redundant dictionaries. Appl Comput Harmon Anal 2011;31:59–73.
[18] Kurokawa U, Choi BI, Chang C-C. Filter-based miniature spectrometers: spectrum reconstruction using adaptive regularization. IEEE Sens J 2011;11:1556–63.
[19] Koh K, Kim S-J, Boyd S. An interior-point method for large-scale l1-regularized logistic regression. J Mach Learn Res 2007;8:1519–55.